

# Two-Dimensional Memristive Hyperchaotic Maps and Application in Secure Communication

Houzhen Li , Student Member, IEEE, Zhongyun Hua , Member, IEEE,  
Han Bao , Student Member, IEEE, Lei Zhu , Mo Chen , Member, IEEE,  
and Bocheng Bao , Member, IEEE

**Abstract**—Continuous memristor has been widely used in chaotic oscillating circuits and neuromorphic computing systems. However, discrete memristor and its coupling discrete map have not been noticed yet. This article presents a discrete memristor and constructs a general two-dimensional memristive map model by coupling the discrete memristor with an existing discrete map. The pinched hysteresis loops of the discrete memristor are demonstrated. Four examples of memristive discrete maps are provided and their coupling strength-relied and memristor initial-boosted complex dynamics are investigated using numerical measures. The evaluation results manifest that the discrete memristor can enhance the chaos complexity and its coupling maps can generate hyperchaos. Particularly, the hyperchaotic sequences can nondestructively be controlled by memristor initial state and the initial-controlled hyperchaos is robust, which is applicable to many chaos-based applications. Additionally, we develop a hardware platform to implement the memristive maps and acquire the four-channel hyperchaotic sequences. We also apply the memristive maps to the application of secure communication and the experiments show that the memristive maps display better performance than some existing discrete maps.

**Index Terms**—Chaos, discrete memristor, hardware platform, hyperchaotic sequence, memristive map, secure communication.

## I. INTRODUCTION

MEMRISTOR can be treated as an organic link between the electric field and magnetic field in the quasistatic

Manuscript received May 13, 2020; revised July 30, 2020; accepted August 31, 2020. Date of publication September 15, 2020; date of current version June 28, 2021. This work was supported in part by the National Natural Science Foundations of China under Grant 51777016, Grant 61701137, and Grant 61801054, and in part by the Natural Science Foundation of Jiangsu Province, China, under Grant BK20191451. (*Corresponding authors: Bocheng Bao; Zhongyun Hua.*)

Houzhen Li, Han Bao, Mo Chen, and Bocheng Bao are with the School of Microelectronics and Control Engineering, Changzhou University, Changzhou 213164, China (e-mail: leehzh@126.com; hi@charlesbao.com; mchen@cczu.edu.cn; mervinbao@126.com).

Zhongyun Hua is with the School of Computer Science and Technology, Harbin Institute of Technology, Shenzhen, Shenzhen 518055, China (e-mail: huazym@gmail.com).

Lei Zhu is with the School of Electrical and Information Engineering, Jiangsu University of Technology, Changzhou 213001, China (e-mail: zhuleei@126.com).

Color versions of one or more of the figures in this article are available online at <https://ieeexplore.ieee.org>.

Digital Object Identifier 10.1109/TIE.2020.3022539

expansion of well-known Maxwell's equations [1]. As a special nonlinear circuit component, the resistance or conductance of the memristor can be memorized by regulating the electric charge or magnetic flux [2]. Actually, the electric charge and magnetic flux are the internal attributes for characterizing the basic circuit components [3]. Because of this special nonlinearity, the memristor brings a new direction for the development of chaotic oscillating circuits and their physical applications [4], [5]. Meanwhile, with the synaptic plasticity, the memristor is becoming a basic building block for the implementation of neuromorphic computing systems [6], [7].

Chaotic behaviors can be demonstrated using various continuous and discrete nonlinear dynamical systems under specific control parameters and initial states [5]. A chaotic system generally has many characteristics, including initial state sensitivity, topological transitivity, and periodic orbit density [8], [9]. Thanks to these unique characteristics, the chaotic systems have been deeply studied in academic fields [10]–[12] and extensively applied in industrial fields [13]–[16]. Usually taken as a nonlinear circuit component, the memristor can be readily employed into various existing dynamical circuits and systems to generate complex chaotic oscillations. Many research reports have pointed out that the initial-dependent multistability with coexisting multistable states is relatively easy to emerge in these memristor-based circuits and systems due to the existence of memristors [4], [5].

Multistability, i.e., the coexistence of multiple disconnected attractors, is an intrinsic property of many nonlinear dynamical systems [17]. Some examples of such nonlinear dynamical systems include the initials-dependent dynamical system [18], locally active memristor-based chaotic circuit [19], memristive neuron model with threshold electromagnetic induction [20], simple offset-boostable chaotic system [21], two-dimensional (2-D) sine map with initials-boosted coexisting chaos [11], and multilevel-controlled dc–dc converter [22]. For a chaotic system with multistability, its long-time motion behavior is essentially different and relies on which attraction basin the initial state belongs to. The coexisting multiple-stable states can provide a great flexibility for many chaos-based applications [5]. But it is meaningful to appropriately control the multistability such that the chaotic system can work in a desired steady state.

Because of the existence of infinite equilibrium points, two approaches of achieving the multistability were presented by introducing memristors into the dynamical circuits or systems

[5] and by drawing periodic functions into the offset-boostable systems [21]. Recently, a new mixed approach was proposed by introducing memristors with sine/cosine memductances into the offset-boostable dynamical systems [23]. However, all these approaches were applied to continuous dynamical systems. So applying these approaches to achieving the multistability to discrete maps is attractive. More recently, we discussed how to discretize the continuous memristor by sampling switch [24], and obtained a preliminary and beneficial idea for the discretization of the continuous memristor. Inspired by these scientific considerations, this article presents a discrete memristor and constructs a general 2-D memristive map model by coupling the discrete memristor with an existing 1-D discrete map. Similar to the dynamical effects reported in [25], four examples of the general 2-D memristive map model are provided to exhibit that the discrete memristor can effectively enhance the chaos complexity of the 1-D discrete map.

In fact, the nanoscale implementation of memristors has led to considerable interest in academic and industrial fields [26]. As with the continuous memristor, the newly presented discrete memristor can be broadly used in the chaotic oscillations and neuromorphic computations as well. As a result, designing the discrete memristor-based hyperchaotic maps is a research topic with theoretical significances and application values. Besides, to implement these memristive maps, a hardware platform is developed and the four-channel hyperchaotic sequences are acquired. To explore the application in secure communication, the presented memristive maps are applied to design the reference-modulated differential chaos shift keying (RM-DCSK) [27]. Performance analyses show that the RM-DCSK using these four 2-D memristive maps has much smaller bit error rates (BERs) than using some 1-D chaotic maps.

The rest of this article is organized as follows. Section II presents a discrete memristor and constructs a general 2-D memristive map model. Section III studies four examples of the memristive maps and evaluates the performance of the generated hyperchaotic sequences. Section IV elaborates the mechanism of memristor initial-boosted dynamics and obtains the memristor's initial-controlled hyperchaotic sequences. Section V implements the memristive hyperchaotic maps in a hardware platform and Section VI applies them to the application of secure communication. Finally, Section VII concludes this article.

## II. DISCRETE MEMRISTOR AND ITS COUPLING MAPS

This section presents a discrete memristor with cosine memristance and constructs a general 2-D memristive discrete map model by coupling the discrete memristor with an existing 1-D discrete map.

### A. Discrete Memristor With Cosine Memristance

Following the definition of continuous-time memristor dubbed by Chua in [2], an ideal charge-controlled memristor for the current  $i(t)$  and voltage  $v(t)$  is characterized by

$$\begin{aligned} v(t) &= M(q) \cdot i(t) = \cos q(t) \cdot i(t) \\ dq(t)/dt &= i(t) \end{aligned} \quad (1)$$

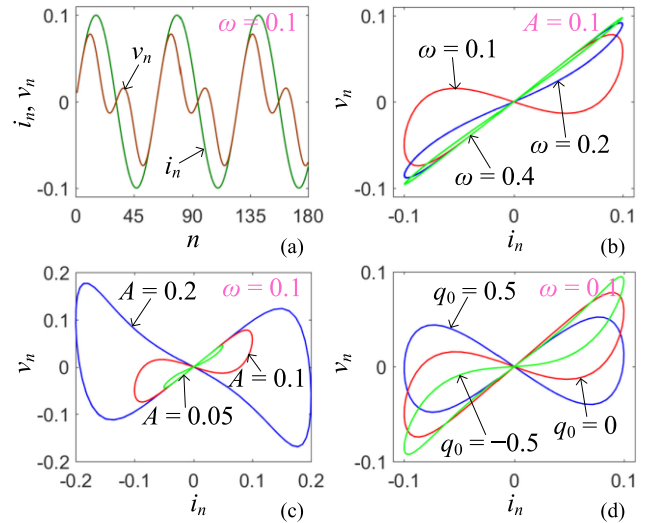


**Fig. 1.** Discrete memristor property when applying the current  $i_n = A \sin(\omega n)$ . (a) Input and output iterative sequences at  $A = 0.1$ ,  $\omega = 0.1$ , and  $q_0 = 0$ . (b) Stimulus frequency-dependent pinched hysteresis loops for  $\omega = 0.1$ ,  $0.2$ , and  $0.4$  with fixed  $A = 0.1$  and  $q_0 = 0$ . (c) Stimulus amplitude-dependent pinched hysteresis loops for  $A = 0.05$ ,  $0.1$ , and  $0.2$  with fixed  $\omega = 0.1$  and  $q_0 = 0$ . (d) Initial state-dependent pinched hysteresis loops for  $q_0 = 0.5$ ,  $0$ , and  $-0.5$  with fixed  $A = 0.1$  and  $\omega = 0.1$ .

where  $q$  is an inner charge variable and  $M(q) = \cos q(t)$  is a periodically varied memristance function. Similar to the ideal flux-controlled memristor with the cosine memductance reported in [23], the charge-controlled memristor in (1) can exhibit a pinched hysteresis loop when applying a bipolar sinusoidal current.

Denote  $i_n$ ,  $v_n$ , and  $q_n$  as the values of current  $i(t)$ , voltage  $v(t)$ , and charge  $q(t)$  at the  $n$ th iteration, respectively. Based on the forward Euler difference method and preliminary idea for discretizing continuous memristor [24], the constitutive relation of the memristor given in (1) can be converted into

$$\begin{aligned} v_n &= M(q_n) \cdot i_n = \cos q_n \cdot i_n \\ q_{n+1} &= q_n + h \cdot i_n \end{aligned} \quad (2)$$

where  $q_{n+1}$  is the value of charge  $q(t)$  at the  $(n+1)$ th iteration and  $h$  is an iteration step size. Without the loss of generality, denote the iteration step size as  $h = 1$ . Therefore, a discrete memristor with cosine memristance can be modeled by (2).

To demonstrate the property of the discrete memristor in MATLAB environment, we take a discrete sinusoidal current  $i_n = A \sin(\omega n)$  as the terminal input of the discrete memristor. By fixing  $A = 0.1$ ,  $\omega = 0.1$ , and  $q_0 = 0$ , the iterative sequences of the input  $i_n$  and output  $v_n$  are together plotted in Fig. 1(a). By fixing  $\omega = 0.1$ ,  $0.2$ , and  $0.4$ , and  $A = 0.1$  and  $q_0 = 0$  as well as  $A = 0.05$ ,  $0.1$ , and  $0.2$ , and  $\omega = 0.1$  and  $q_0 = 0$ , the stimulus frequency- and amplitude-dependent pinched hysteresis loops in the  $i_n-v_n$  plane are simulated in Fig. 1(b) and (c), respectively. Furthermore, by fixing  $q_0 = 0.5$ ,  $0$ , and  $-0.5$ , and  $A = 0.1$  and  $\omega = 0.1$ , the inner initial-dependent pinched hysteresis loops in the  $i_n-v_n$  plane are depicted in Fig. 1(d). These numerical results, as given in Fig. 1, perfectly exhibit the unique property

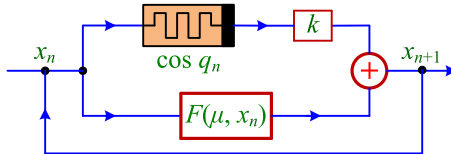


Fig. 2. Structure of the general 2-D memristive map model.

of the discrete memristor that behaves like a memristor in the continuous-time domain [5].

Besides, it is critical that the initial state-dependent pinched hysteresis loops also embody the memory effect of the discrete memristor. With the change of the initial state, the local activity of the discrete memristor is varied, which can impact the dynamical behaviors of its coupling discrete maps.

### B. Two-Dimensional General Memristive Map Model

The logistic map, sine map, and tent map are three well-known 1-D discrete maps. Under typical parameter settings, they can display chaotic behaviors. However, they have simple system structures and their chaotic behaviors thereby may be predicted [28].

To enhance the chaos complexity of these 1-D discrete maps, a general 2-D memristive map model is newly constructed by coupling the discrete memristor given in (2) and an existing 1-D discrete map. Its system structure is shown in Fig. 2, in which  $F(\mu, x_n)$  represents an existing 1-D discrete map with a control parameter  $\mu$ , and  $k$  denotes the coupling strength between the discrete memristor and existing 1-D discrete map. Using such a system structure, some 2-D memristive maps can be derived.

With the system structure in Fig. 2, one can obtain the mathematical equations of the general 2-D memristive map model, which is described as

$$\begin{aligned} x_{n+1} &= F(\mu, x_n) + k \cos q_n \cdot x_n \\ q_{n+1} &= q_n + x_n. \end{aligned} \quad (3)$$

Using (3), the 2-D memristive discrete maps can be yielded by coupling the discrete memristor with some existing 1-D discrete maps. This method is simple but very effective. It can greatly enhance the chaos complexity of these existing 1-D discrete maps and thereby results in the occurrence of complex dynamics in the presented memristive discrete maps.

The stability of a discrete iteration map can be characterized using its fixed points. A fixed point of a map is the point that maps to itself in its domain. The fixed point of the 2-D memristive map, denoted as  $(x^*, q^*)$ , is the solutions of the following equation:

$$\begin{aligned} x^* &= F(\mu, x^*) + k \cos q^* \cdot x^* \\ q^* &= q^* + x^*. \end{aligned} \quad (4)$$

Clearly, two specific cases can be divided.

First, when  $F(\mu, 0) = 0$ , the memristive map model has infinite fixed points and these fixed points can be expressed as

$$S = (x^*, q^*) = (0, \eta) \quad (5)$$

where  $\eta$  represents an arbitrary constant. The characteristic polynomial is deduced from the Jacobian matrix at  $S$  as

$$P(\lambda) = (\lambda - 1)[\lambda - g(\mu) - k \cos \eta] \quad (6)$$

where  $g(\mu) = \partial F(\mu, x_n)/\partial x_n|_{x_n=0}$ . The eigenvalues  $\lambda_1$  and  $\lambda_2$  in (6) are thereby obtained as

$$\lambda_1 = 1, \lambda_2 = g(\mu) + k \cos \eta. \quad (7)$$

If  $|\lambda_1| < 1$  and  $|\lambda_2| < 1$ , the fixed points  $S$  in (5) are stable; otherwise, they are unstable. As can be seen from (7),  $\lambda_1$  is always on the unit circle, whereas  $\lambda_2$  could be inside or outside the unit circle that depends on  $g(\mu)$  and the initial state  $\eta$  of the memristor inner state  $q$ . Therefore, the fixed points for the memristive map model may be unstable or critical stable.

Second, when  $F(\mu, 0) \neq 0$ , the memristive map model has no fixed points. This is because (4) has no real solutions when  $F(\mu, 0) \neq 0$ . In this case, the memristive map model shows the hidden periodic, chaotic, or hyperchaotic oscillation.

## III. TWO-DIMENSIONAL MEMRISTIVE HYPERCHAOTIC MAPS

This section studies four examples of 2-D memristive maps using several numerical measures and evaluates the dynamical performance of the hyperchaotic sequences generated by these memristive maps.

### A. Examples of 2-D Memristive Maps

Three 2-D memristive maps can be yielded from (3) by setting the 1-D chaotic map as the existing logistic map, sine map, or tent map, respectively. The mathematical equations of these 2-D memristive maps are described as

$$\begin{aligned} x_{n+1} &= \mu x_n (1 - x_n) + k \cos q_n \cdot x_n \\ q_{n+1} &= q_n + x_n \end{aligned} \quad (8)$$

with  $F(\mu, 0) = 0$  and  $g(\mu) = \mu$

$$\begin{aligned} x_{n+1} &= \mu \sin(2\pi x_n) + k \cos q_n \cdot x_n \\ q_{n+1} &= q_n + x_n \end{aligned} \quad (9)$$

with  $F(\mu, 0) = 0$  and  $g(\mu) = 2\pi\mu$ , and

$$\begin{aligned} x_{n+1} &= \begin{cases} \mu x_n + k \cos q_n \cdot x_n, & x_n < 0.5 \\ \mu(1 - x_n) + k \cos q_n \cdot x_n, & x_n \geq 0.5 \end{cases} \\ q_{n+1} &= q_n + x_n \end{aligned} \quad (10)$$

with  $F(\mu, 0) = 0$  and  $g(\mu) = \mu$ , respectively. The chaotic models in (8)–(10) are called 2-D memristive logistic map (2D-MLM), 2-D memristive sine map (2D-MSM), and 2-D memristive tent map (2D-MTM), respectively. Moreover, when coupling the discrete memristor with a linear discrete map, a 2-D simple memristive map, namely 2D-SMM, can be extended from (3) as

$$\begin{aligned} x_{n+1} &= \mu x_n + k \cos q_n \cdot x_n \\ q_{n+1} &= q_n + x_n \end{aligned} \quad (11)$$

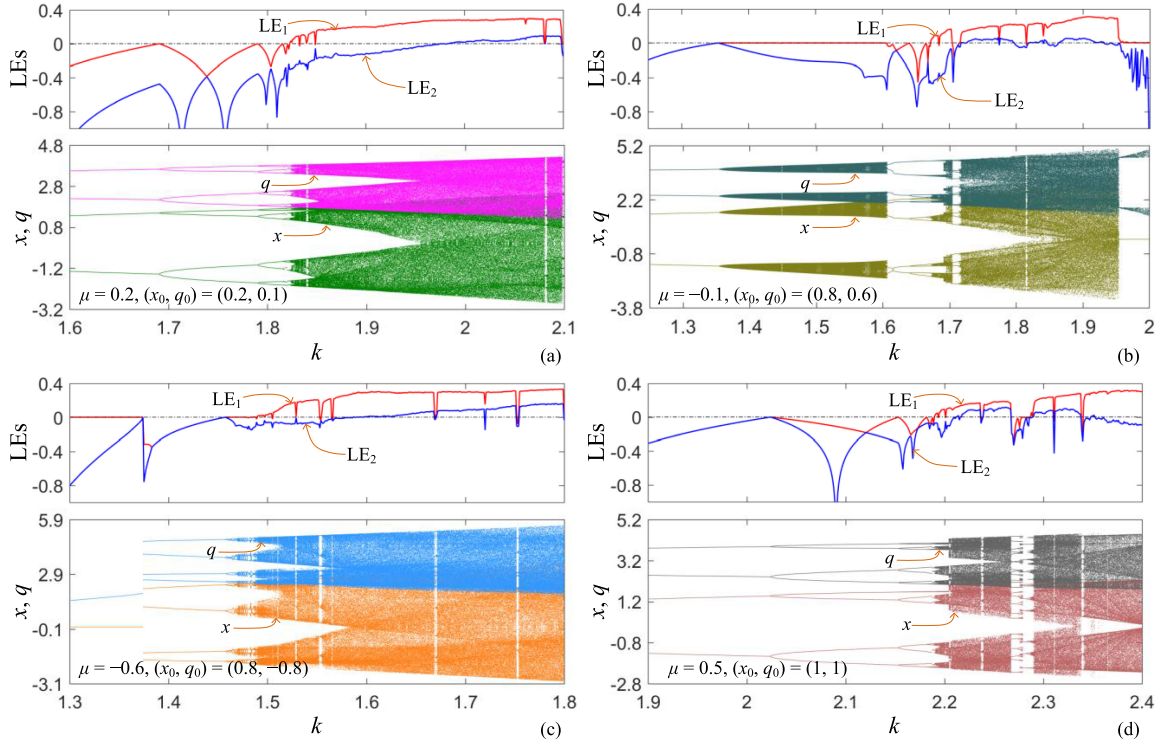


**Fig. 3.** For the memristive maps, the coupling strength-relied bifurcation diagrams of the states  $x$  and  $q$  (bottom) and finite-time LE spectra (top). (a) For  $\mu = 0.2$ ,  $(x_0, q_0) = (0.2, 0.1)$ , and numerical plots of 2D-MLM with  $k \in [1.6, 2.1]$ . (b) For  $\mu = -0.1$ ,  $(x_0, q_0) = (0.8, 0.6)$ , and numerical plots of 2D-MSM with  $k \in [1.25, 2.0]$ . (c) For  $\mu = -0.6$ ,  $(x_0, q_0) = (0.8, -0.8)$ , and numerical plots of 2D-MTM with  $k \in [1.3, 1.8]$ . (d) For  $\mu = 0.5$ ,  $(x_0, q_0) = (1, 1)$ , and numerical plots of 2D-SMM with  $k \in [1.9, 2.4]$ .

with  $F(\mu, 0) = 0$  and  $g(\mu) = \mu$ . Therefore, a total number of four 2-D memristive maps are generated by coupling the discrete memristor with four 1-D discrete maps.

Because  $F(\mu, 0) = 0$  in the aforementioned four 2-D memristive maps, they all have infinite fixed points given in (5). Hence, their eigenvalues at the infinite fixed points can be characterized by the two eigenvalues in (7). Besides, since all these 2-D memristive maps can generate the hyperchaos, they are also called 2-D memristive hyperchaotic maps. Note that the control parameter  $\mu$  and coupling strength  $k$  can be determined according to the eigenvalues in (7), and the numerical plots in Sections III-B and III-C.

### B. Coupling Strength-Relied Bifurcations

When investigating the bifurcation diagrams of the 2-D memristive maps, we set the control parameter  $\mu$  as a determined value and the coupling strength  $k$  as an adjustable bifurcation parameter. For the aforementioned four 2-D memristive maps, the bifurcation diagrams of the states  $x$  and  $q$ , and finite-time Lyapunov exponent (LE) spectra are numerically simulated and demonstrated in Fig. 3, where the representative values of control parameter  $\mu$  and initial states  $(x_0, q_0)$  as well as the adjustable intervals of coupling strength  $k$  are given in details. Note that the LE spectra are computed using the Wolf's Jacobian-based method.

As can be observed from Fig. 3, all the four 2-D memristive maps have hyperchaotic behaviors in the relatively wide parameter intervals and display the complex dynamical behaviors of

**TABLE I**  
TWO-DIMENSIONAL MEMRISTIVE MAPS AND THEIR PARAMETERS, INITIAL STATES, AND LEs

Memristive maps	$(\mu, k)$	$(x_0, q_0)$	LE <sub>1</sub> , LE <sub>2</sub>
2D-MLM	(0.2, 2.08)	(0.2, 0.1)	0.2916, 0.0945
2D-MSM	(-0.1, 1.88)	(0.8, 0.6)	0.2683, 0.0512
2D-MTM	(-0.6, 1.78)	(0.8, -0.8)	0.3226, 0.1507
2D-SMM	(0.5, 2.33)	(1, 1)	0.2681, 0.0931

period/quasiperiod, chaos, and periodic windows. In particular, both the 2D-MLM in Fig. 3(a) and 2D-SMM in Fig. 3(d) have the route to chaos in the same period-doubling way with the change of their coupling strengths, whereas both the 2D-MSM in Fig. 3(b) and 2D-MTM in Fig. 3(c) have the route to chaos in the same quasi-periodic way with the increment of their coupling strengths and can show quasi-periodic behaviors in different parameter intervals.

### C. Representative Hyperchaotic Attractors

The representative parameters, initial states, and related LEs (LE<sub>1</sub> and LE<sub>2</sub>) of the four 2-D memristive maps are summarized in Table I. One can see that all the four 2-D memristive maps have two positive LEs under these parameter and initial state settings. This indicates that all these 2-D memristive maps are hyperchaotic.

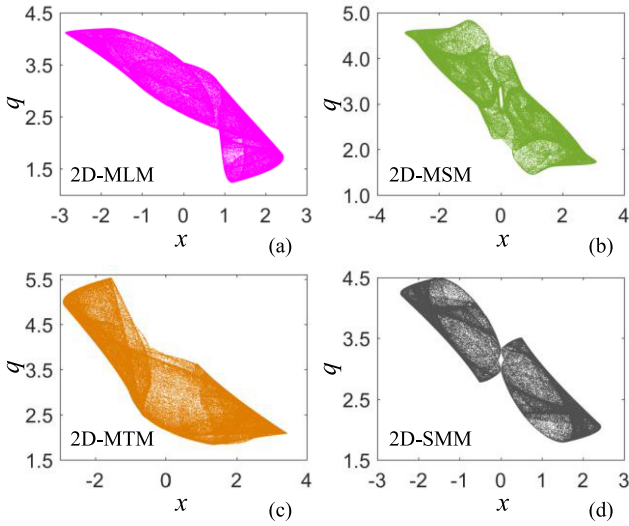


**Fig. 4.** Phase plane plots of the representative hyperchaotic attractors for the four 2-D memristive maps. (a) 2D-MLM with  $\mu = 0.2$ ,  $k = 2.08$ , and  $(x_0, q_0) = (0.2, 0.1)$ . (b) 2D-MSM with  $\mu = -0.1$ ,  $k = 1.88$ , and  $(x_0, q_0) = (0.8, 0.6)$ . (c) 2D-MTM with  $\mu = -0.6$ ,  $k = 1.78$ , and  $(x_0, q_0) = (0.8, -0.8)$ . (d) 2D-SMM with  $\mu = 0.5$ ,  $k = 2.33$ , and  $(x_0, q_0) = (1, 1)$ .

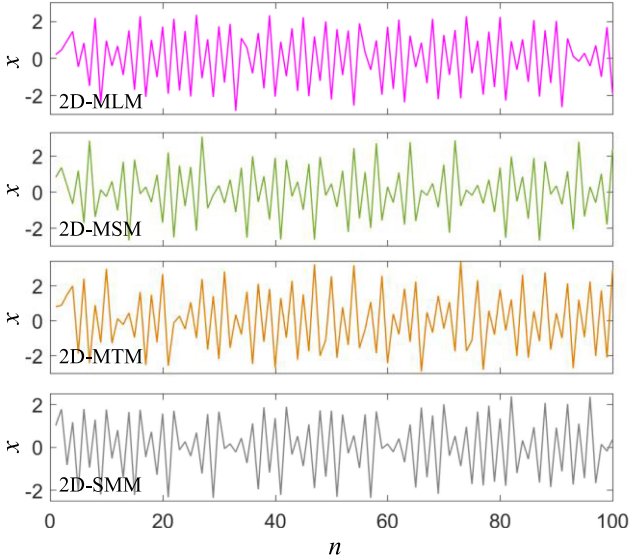


**Fig. 5.** Hyperchaotic sequences generated by the four 2-D memristive maps under the representative parameters and initial states listed in Table I.

The phase plane plots of the four 2-D memristive maps under these representative parameters and initial state settings listed in Table I are obtained and displayed in Fig. 4. One can observe, all hyperchaotic attractors possess complicated fractal structure. The hyperchaotic attractor in Fig. 4(a) or (c) is merged into one complete piece, whereas that in Fig. 4(b) or (d) is constructed by two partially connected pieces. Correspondingly, the generated hyperchaotic sequences for the four 2-D memristive maps are depicted in Fig. 5, which are all disordered and aperiodic, suitable for developing the application in the field of information industry.

**TABLE II**  
PERFORMANCE FOR HYPERCHAOTIC SEQUENCES OF  
2-D MEMRISTIVE MAPS

Memristive maps	PE	SE	CorDim	$D_{KY}$
2D-MLM	3.9037	0.8247	1.5849	2.0
2D-MSM	3.4872	0.7511	1.5137	2.0
2D-MTM	4.1438	0.8573	1.6574	2.0
2D-SMM	3.4478	0.6539	1.5440	2.0

$D_{KY}$ : Kaplan–Yorke dimension.

The performance of the hyperchaotic sequences that emerged from the 2-D memristive maps is evaluated using the permutation entropy (PE) [29], spectral entropy (SE) [23], correlation dimension (CorDim) [30], and Kaplan–Yorke dimension [31]. The length of all hyperchaotic sequences is determined as  $10^5$  and the computed results for these four hyperchaotic sequences, as depicted in Fig. 5, are listed in Table II. As shown, these hyperchaotic sequences have the outstanding performance indicators, which allow the 2-D memristive maps to be applicable to many chaos-based applications. This indicates that the introducing discrete memristor can greatly enhance the chaos complexity of the original 1-D discrete map.

#### IV. MEMRISTOR INITIAL-BOOSTED DYNAMICS

Combined with the discrete memristor, the presented 2-D memristive maps have infinite fixed points, resulting in the coexistence of infinite attractors by the memristor initial boosting.

##### A. Memristor Initial-Boosting Mechanism

To demonstrate the dynamical mechanism of memristor initial-boosted behavior, the 2-D memristive map model in (3) can be rewritten as the following iterated equation form:

$$x_{n+1} = F(\mu, x_n) + k \cos \left( q_0 + \sum_{l=1}^{n-1} x_l \right) \cdot x_n. \quad (12)$$

For an integer number  $m$ , denote

$$q_0 = q_{00} + 2m\pi \quad (13)$$

where  $q_{00}$  is a compensation initial state that satisfies the following requirement:

$$-\pi < q_{00} + \sum_{l=1}^{n-1} x_l < \pi. \quad (14)$$

Thus, one has

$$\cos \left( q_0 + \sum_{l=1}^{n-1} x_l \right) = \cos \left( q_{00} + \sum_{l=1}^{n-1} x_l \right). \quad (15)$$

The result in (15) demonstrates the cyclic property of the cosine memristance in (2).

The map model described by the difference equation in (12) is cyclic about the memristor initial state  $q_0$ . The cyclic property can be proved from the invariance of the map model (12) by the linear transformation (13). It turns out that the dynamical

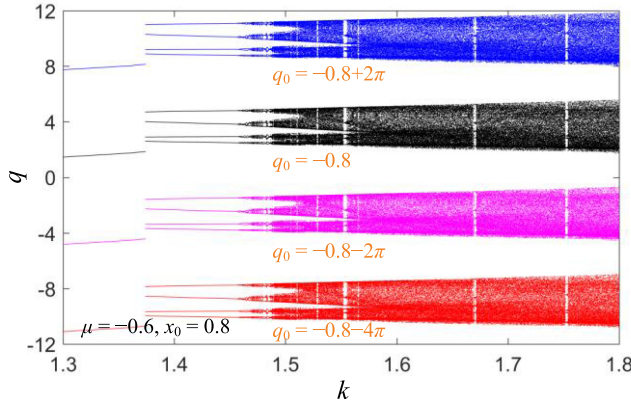


**Fig. 6.** For  $\mu = -0.6$ ,  $x_0 = 0.8$ , and  $q_0 = -0.8 + 2m\pi$  ( $m = -2, -1, 0, 1$ ) with  $k \in [1.3, 1.8]$ , memristor initial-boosted bifurcation diagrams along the  $q$ -axis.

behaviors of the 2-D memristive maps are cyclically changed with the periodic evolution of the memristor initial state  $q_0$  with period  $2\pi$ . Therefore, the 2-D memristive map described by (3) is a boostable map induced by the memristor initial state along the memristor state direction.

### B. Memristor Initial-Boosted Bifurcations

Take 2D-MTM as an example to exhibit the memristor initial-boosted bifurcation behaviors. For the sake of intuition, the coupling strength-relied bifurcation diagrams of the memristor state  $q$  of 2D-MTM are numerically simulated under some specific memristor initial states, as shown in Fig. 6, where  $\mu = -0.6$ ,  $x_0 = 0.8$ ,  $q_0 = -0.8 + 2m\pi$  ( $m = -2, -1, 0, 1$ ), and  $k \in [1.3, 1.8]$ . One can find that the bifurcation diagrams for these specific memristor initial states have the same bifurcation structure. This means that the coupling strength-relied bifurcation behaviors can be completely boosted in the dynamic amplitudes by the memristor initial states with period  $2\pi$ , which well verify the feasibility of the aforementioned theoretical analysis. Particularly, when  $m$  goes to infinity, infinitely many memristor initial-boosted bifurcations are emerged on the dimension  $q$ , leading to the coexistence of infinitely many attractors in 2D-MTM.

As illustrated in Table I and Figs. 4 and 5, the representative parameters of 2D-MTM are determined as  $\mu = -0.6$  and  $k = 1.78$ . To inspect the dynamical effects of each initial state in 2D-MTM, we draw the local attraction basin in the  $x_0-q_0$  plane and show the result in the bottom of Fig. 7. Meanwhile, an example of the memristor initial-relied bifurcation diagram for fixed  $x_0 = 0.8$  is considered and the result is plotted at the top of Fig. 7. As can be seen, the local attraction basin has complex manifold structures and basin boundaries, and the color-painted blocks labeled from  $m = -3$  to  $m = 2$  indicate six attracting regions of hyperchaotic attractors that are  $2\pi$  apart from each other. In addition, the yellow region represents the stable point attractor and the white region stands for the unbounded behavior. The numerical results in Fig. 7 manifest that the dynamical behaviors in 2D-MTM are strongly relied on the initial state

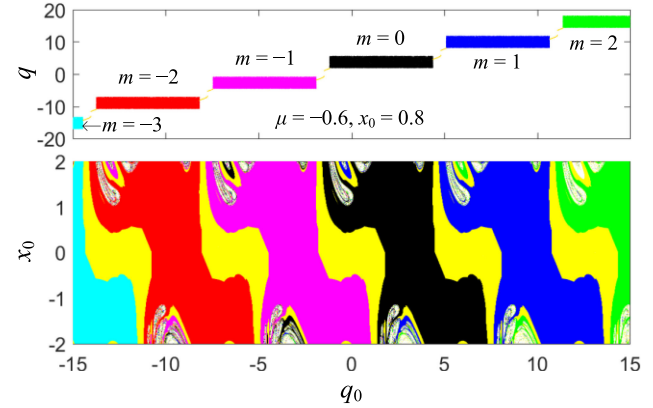


**Fig. 7.** For  $\mu = -0.6$  and  $k = 1.78$ , the local attraction basin with  $q_0 \in [-15, 15]$  and  $x_0 \in [-2, 2]$  (bottom), and memristor initial-relied bifurcation diagram of the memristor state  $q$  with fixed  $x_0 = 0.8$  (top).

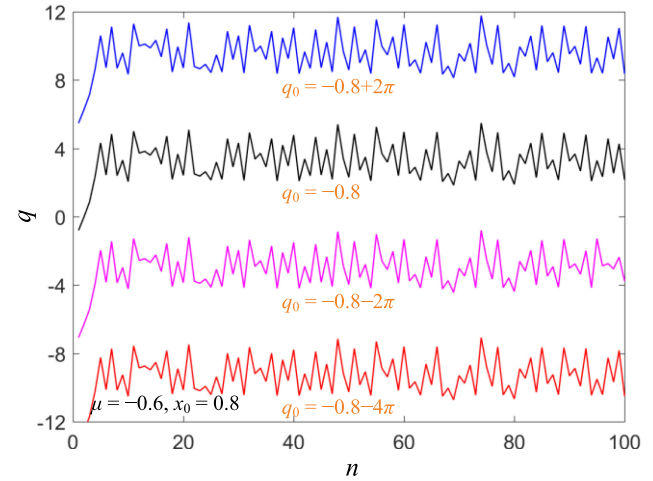


**Fig. 8.** Memristor initial-controlled hyperchaotic sequences of 2D-MTM, demonstrating the amplitude-switched robust hyperchaos by the memristor initial state.

of the memristor. These fantastic results can be extended to the other 2-D memristive hyperchaotic maps as well.

### C. Memristor Initial-Controlled Hyperchaotic Sequences

Following the results given in Figs. 6 and 7, the hyperchaotic sequences generated from 2D-MTM under the specific parameter settings can be controlled in the dynamic amplitudes by the memristor initial states with period  $2\pi$ . For fixed  $\mu = -0.6$ ,  $k = 1.78$ , and  $x_0 = 0.8$ , when the memristor initial states are set to  $q_0 = -0.8 + 2m\pi$  ( $m = -2, -1, 0, 1$ ), four hyperchaotic sequences are generated from 2D-MTM, which are plotted in Fig. 8. The numerical results imply that the dynamic amplitudes of the hyperchaotic sequences can be controlled by switching the memristor initial states.

Similar to the hyperchaotic sequences of the 2-D memristive maps, the performance of the memristor initial-controlled hyperchaotic sequences generated from the 2D-MTM can be

**TABLE III**  
PERFORMANCE FOR INITIAL-CONTROLLED HYPERCHAOTIC SEQUENCES

$q_0$	LE <sub>1</sub> , LE <sub>2</sub>	PE	SE	CorDim
$-0.8+2\pi$	0.3227, 0.1502	4.1299	0.8583	1.6598
-0.8	0.3226, 0.1507	4.1438	0.8573	1.6574
$-0.8-2\pi$	0.3198, 0.1506	4.1298	0.8576	1.6581
$-0.8-4\pi$	0.3232, 0.1529	4.1382	0.8583	1.6533

evaluated by employing the Wolf's Jacobian-based LEs (LE<sub>1</sub> and LE<sub>2</sub>), PE [29], SE [23], and CorDim [30] as well. The computed results for the four hyperchaotic sequences in Fig. 8 are listed in Table III. As can be observed, the memristor initial-controlled hyperchaotic sequences have almost the same values for different performance indicators. The tiny differences are caused by numerical simulation errors. This indicates that the hyperchaotic sequences generated from the 2D-MTM can be nondestructively controlled by the memristor initial state and that the memristor initial-controlled hyperchaos is robust.

## V. HARDWARE IMPLEMENTATION

This section implements the 2-D memristive hyperchaotic maps in a hardware platform.

Based on a pony-size and low-cost microcontroller, a hardware platform is developed to implement the 2-D memristive hyperchaotic maps. The hardware platform contains 16-bit microcontroller MSP430F149, 12-bit D/A converter TLV5638, and other peripheral circuits. The microcontroller is used for implementing the 2-D memristive hyperchaotic maps and the D/A converter provides the corresponding analog voltage signals.

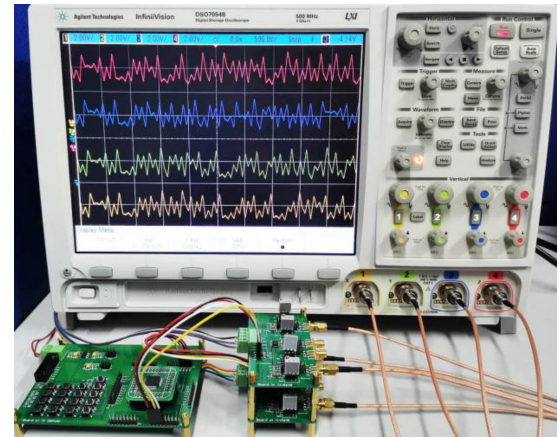
According to the four mathematical models given by (8)–(11), we first implement the 2-D memristive hyperchaotic maps using C language and then download the software codes to the microcontroller. The parameters and initial states are set as the representative values given in Tables I and III. After preloading the representative parameters and initial states to the hardware platform, and running the program software in the microcontroller, the four-channel hyperchaotic voltage signals of the 2-D memristive hyperchaotic maps can be synchronously generated.

Fig. 9 shows the snapshot of our experimental prototype. Corresponding to the numerical results shown in Figs. 5 and 8, the generated four-channel hyperchaotic voltage signals are displayed on the digital oscilloscope, as shown in Fig. 10. It shows that two sets of four-channel hyperchaotic sequences oscillate in different dynamic ranges that are preprocessed by the software. The experimental results demonstrate the feasibility of the hardware implementation for the presented 2-D memristive hyperchaotic maps.

## VI. APPLICATION OF SECURE COMMUNICATION

This section applies the 2-D memristive hyperchaotic maps to secure communication.

Since the chaotic systems have the properties of ergodicity and unpredictability, they can be used to securely transmit data



**Fig. 9.** Experimental prototype of the microcontroller-based hardware platform and captured four-channel hyperchaotic sequences of 2D-MTM.

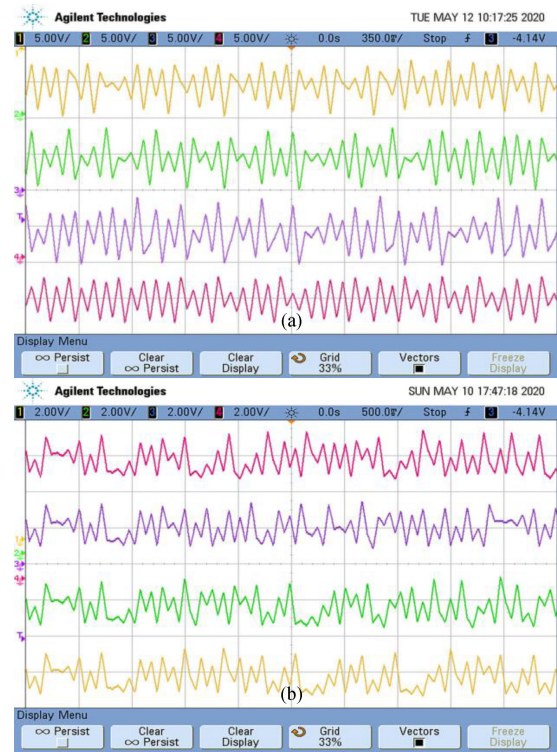


**Fig. 10.** Experimentally measured hyperchaotic sequences from the hardware platform. (a) Hyperchaotic sequences generated by four 2-D memristive maps. (b) Memristor initial-controlled hyperchaotic sequences of 2D-MTM.

[32]. When chaotic systems are used in secure communication, their dynamical performance highly determines the transmission performance. Because our 2-D memristive hyperchaotic maps have complex dynamical properties, they are suitable for this application. To demonstrate this property, we apply them to a secure communication scheme, i.e., the RM-DCSK [27], and investigate the performance of the communication scheme in defending the transmission noise.

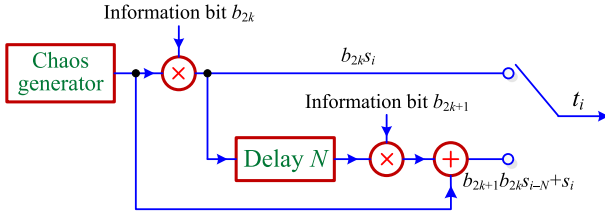


Fig. 11. Structure of the sender in the RM-DCSK.

The RM-DCSK includes the sender and receiver parts. The detailed structure of the sender of the RM-DCSK is plotted in Fig. 11. The chaos generator is a chaotic system and it generates chaotic sequences with given initial states. One part of chaotic sequences is directly encoded with the information bits and the other part of chaotic sequences is combined with the encoded results. Then the final transmitted signal is generated by switching the time. The mathematical description about the generation of the transmitted signal is as follows. Suppose  $S_k$  is an  $N$ -length chaotic sequence and  $S_k = \{s_i | 2kN < i \leq (2k+1)N\}$ , where  $N$  is an integer number called the spread factor. Then the transmitted signal in the  $k$ th frame can be generated as

$$t_i = \begin{cases} b_{2k}s_i, & 2kN < i \leq (2k+1)N \\ b_{2k+1}b_{2k}s_{i-N} + s_i, & (2k+1)N < i \leq 2(k+1)N \end{cases} . \quad (16)$$

The chaotic output  $s_i$  has the property that

$$s_{(2k+1)N+m} = s_{2(k+1)N+m}, \forall k \in \{0, \pm 1, \pm 2, \dots\}. \quad (17)$$

From the generation process of the transmitted signal, one frame embeds two bits of information. The first bit is encoded using an  $N$ -length chaotic sequence  $S_k$  directly, while the second bit is encoded using the chaotic sequence  $S_k$  and  $S_{k+1}$ . Because the sender encodes the information in a continuous way, an  $N$  delay is required when encoding two bits of information in one frame.

The receiver decodes the received signal from the sender. Since most of the physical transmission channels are noisy channels, the received signals may be blurred by the noise and thereby is different from the transmitted signals in the sender. Suppose the recovered signal  $r_i$  is represented as  $r_i = t_i + n_i$ , where  $n_i$  is the noise part. The correlator  $C_m$  for decoding the information bit  $b_m$  is calculated by adding the multiplication of  $r_i$  with its  $N$  delayed value, namely

$$C_m = \sum_{i=mN+1}^{(m+1)N} r_i r_{i-N}. \quad (18)$$

Thus, the correlator for the information bit  $b_{2k}$  is calculated as

$$\begin{aligned} C_{2k} &= \sum_{i=2kN+1}^{(2k+1)N} (t_i + n_i)(t_{i-N} + n_{i-N}) \\ &= \sum_{i=2kN+1}^{(2k+1)N} (b_{2k}s_i + n_i)(b_{2k-1}b_{2(k-1)}s_{i-2N} + s_{i-N} + n_{i-N}). \end{aligned} \quad (19)$$

In view of the fact that  $s_{i-N} = s_i$  in the encoding process, the above-mentioned correlator can be rewritten as

$$\begin{aligned} C_{2k} &= \sum_{i=2kN+1}^{(2k+1)N} (b_{2k}s_i + n_i)(b_{2k-1}b_{2(k-1)}s_{i-2N} + s_i + n_{i-N}) \\ &= b_{2k} \sum_{i=2kN+1}^{(2k+1)N} s_i^2 + R(n_i, n_{i-N}) \end{aligned} \quad (20)$$

where  $R(n_i, n_{i-N})$  is the remainder and

$$\begin{aligned} R(n_i, n_{i-N}) &= \sum_{i=2kN+1}^{(2k+1)N} (b_{2k}b_{2k-1}b_{2(k-1)}s_i s_{i-2N} + b_{2k}s_i n_{i-N}) \\ &\quad + \sum_{i=2kN+1}^{(2k+1)N} (b_{2k-1}b_{2(k-1)}s_{i-2N}n_i + s_i n_i + n_i n_{i-N}). \end{aligned} \quad (21)$$

Because the chaotic sequence  $s_i$  is uniformly distributed and the noise has far less energy than the transmitted data, the remainder  $R(n_i, n_{i-N})$  contributes less to the sign of the correlator  $C_{2k}$  than the information part. Then the sign of the correlator is determined by the transmitted bit  $b_{2k}$ . Similarly, the signal of  $C_{2k+1}$  is determined by the transmitted bit  $b_{2k+1}$ . Thus, the bit  $b_m$  can be decoded as

$$b_m = \begin{cases} 1, & \text{if } C_m > 0 \\ -1, & \text{if } C_m \leq 0 \end{cases} . \quad (22)$$

Our experiments use the four presented memristive hyperchaotic maps as the chaos generator to simulate the RM-DCSK. Because most of the physical transmission channels contain the Gaussian noise, we simulate the RM-DCSK in the additive white Gaussian noise environment, and calculate the BERs of the RM-DCSK in different noise strengths and spread factors. The initial states and control parameters  $(x_0, q_0, \mu, k)$  for the presented 2D-MLM, 2D-MSM, 2D-MTM, and 2D-SMM are set as  $(0.2, 0.1, 0.2, 2.08)$ ,  $(0.8, 0.6, -0.1, 1.88)$ ,  $(0.8, -0.8, -0.6, 1.78)$ , and  $(1, 1, 0.5, 2.33)$ , respectively, while the initial states and control parameters  $(x_0, \mu)$  for the classical logistic, sine, and tent maps are set as  $(0.2, 3.68)$ ,  $(0.2, 0.93)$ , and  $(0.2, 1.49)$ . These parameter settings can ensure that all the discrete maps have chaotic behaviors.

Two groups of experiments are tested. The first group tests the BERs of the RM-DCSK in different noise strengths. Specifically, simulate the RM-DCSK using every chaotic map under the signal-noise-rate (SNR) strength  $\text{SNR} \in \{0, 1, 2, \dots, 30\}$  by fixing the spread factor  $N = 50$ , and then calculate the BERs between the decoded data in the receiver and the encoded data in the sender. Fig. 12(a) shows the experimental results. As shown, when the noise strength is strong, the RM-DCSK using all the chaotic maps can achieve the similar BERs, with the increment of the SNR, the proposed 2D-MLM, 2D-MSM, 2D-MTM, and 2D-SMM can achieve far smaller BERs than the three classical 1-D chaotic maps. The other group of experiments tests the BERs of the RM-DCSK in different spread factor  $N$ . Specifically, simulate the RM-DCSK using every chaotic map when the spread factor  $N \in \{10, 20, \dots, 100\}$  by fixing the noise strength  $\text{SNR} = 25$ , and then calculate the BERs between the decoded data and

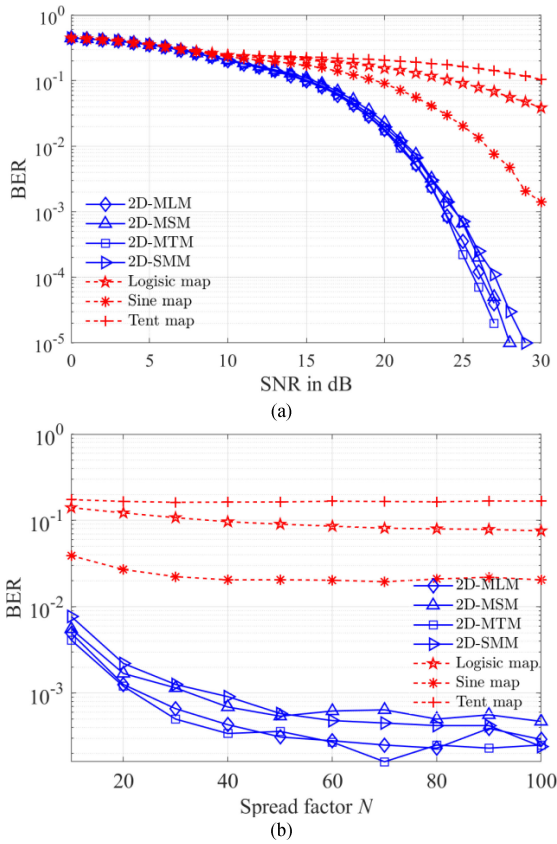


**Fig. 12.** BERs of the RM-DCSK using different chaotic maps when (a) spread factor  $N = 50$  and noise strength  $\text{SNR} \in \{0, 1, 2, \dots, 30\}$ , and (b)  $\text{SNR} = 25$  and  $N \in \{10, 20, \dots, 100\}$ .

the encoded data. Fig. 12(b) plots the experimental results. One can observe that the RM-DCSK using the presented 2-D memristive hyperchaotic maps can obtain much smaller BERs than using the existing 1-D chaotic maps. To be sure, when applying the chaotic maps in secure communication, the distribution of the generated chaotic sequences can greatly affect the transmission efficiency. Since the 2-D memristive hyperchaotic maps have quite complex dynamics, they can generate chaotic sequences with uniform distribution. Thus, they are more suitable for the secure communication application than some 1-D chaotic maps.

## VII. CONCLUSION

The memristor is a fundamental circuit component with special nonlinearity and synaptic plasticity. While introducing the memristor into a chaotic oscillating circuit, the memristor can make the circuit achieve complex dynamics, such as initial-dependent multistability. To extend the memristor to discrete chaotic systems, this article presented a discrete memristor and constructed four 2-D memristive hyperchaotic maps by coupling the discrete memristor with four existing 1-D discrete maps. Because of the existence of the infinite fixed points, these 2-D memristive maps could exhibit the coupling strength-relied and memristor initial-boosted complex dynamics. The analysis results showed that the discrete memristor could enhance the chaos complexity and these 2-D memristive maps could generate the hyperchaos. Notably, the hyperchaotic sequences

could nondestructively be controlled by the memristor initial state. These properties allow the memristive hyperchaotic maps to have many application merits. Besides, a hardware platform was developed to implement these memristive maps. It could synchronously provide the four-channel hyperchaotic voltage signals. To demonstrate their applications, these memristive maps were applied to designing RM-DCSK. The performance analyses showed that the memristive maps were suitable for the application of secure communication. With the outstanding performance indicators, these generated hyperchaotic sequences can also be used for designing the pseudorandom numbers (PRNs) with high randomness [11], [33]. Of course, it is well worth studying the applications of the discrete memristor and memristive map-based PRNs in many other information industry scenarios, such as image encryptions [34] and secure communications.

## REFERENCES

- [1] K. Eshraghian *et al.*, "Memristive device fundamentals and modeling: Applications to circuits and systems simulation," *Proc. IEEE*, vol. 100, no. 6, pp. 1991–2007, Jun. 2012.
- [2] L. Chua, "If it's pinched it's a memristor," *Semicond. Sci. Technol.*, vol. 29, no. 10, Sep. 2014, Art. no. 104001.
- [3] F. Z. Wang, "A triangular periodic table of elementary circuit elements," *IEEE Trans. Circuits Syst. I, Reg. Papers*, vol. 60, no. 3, pp. 616–623, Mar. 2013.
- [4] F. Corinto and M. Forti, "Memristor circuits: Bifurcations without parameters," *IEEE Trans. Circuits Syst. I, Reg. Papers*, vol. 60, no. 3, pp. 616–623, Mar. 2013.
- [5] M. Chen, M. Sun, H. Bao, Y. Hu, and B. Bao, "Flux-charge analysis of two-memristor-based Chua's circuit: Dimensionality decreasing model for detecting extreme multistability," *IEEE Trans. Ind. Electron.*, vol. 67, no. 3, pp. 2197–2206, Mar. 2020.
- [6] M. Hu, H. Li, Y. Chen, Q. Wu, G. S. Rose, and R. W. Linderman, "Memristor crossbar-based neuromorphic computing system: A case study," *IEEE Trans. Neural Netw. Learn. Syst.*, vol. 25, no. 10, pp. 1864–1878, Oct. 2014.
- [7] M. Prezioso, F. Merrikh-Bayat, B. D. Hoskins, G. C. Adam, K. K. Likharev, and D. B. Strukov, "Training and operation of an integrated neuromorphic network based on metal-oxide memristors," *Nature*, vol. 521, no. 7550, pp. 61–64, 2015.
- [8] Z. Hua and Y. Zhou, "Exponential chaotic model for generating robust chaos," *IEEE Trans. Syst., Man., Cybern., Syst.*, to be published.
- [9] C. Li, D. Lin, J. Lü, and F. Hao, "Cryptanalyzing an image encryption algorithm based on autoblocking and electrocardiography," *IEEE MultiMedia*, vol. 25, no. 4, pp. 46–56, Oct./Dec. 2018.
- [10] S. Luo and Y. Song, "Chaos analysis-based adaptive backstepping control of the microelectromechanical resonators with constrained output and uncertain time delay," *IEEE Trans. Ind. Electron.*, vol. 63, no. 10, pp. 6217–6225, Oct. 2016.
- [11] H. Bao, Z. Hua, N. Wang, L. Zhu, M. Chen, and B.-C. Bao, "Initials-boosted coexisting chaos in a 2D Sine map and its hardware implementation," *IEEE Trans. Ind. Informat.*, to be published.
- [12] L. Yin, Z. Deng, B. Huo, and Y. Xia, "Finite-time synchronization for chaotic gyros systems with terminal sliding mode control," *IEEE Trans. Syst., Man., Cybern., Syst.*, vol. 49, no. 6, pp. 1131–1140, Jun. 2019.
- [13] X. Meng, P. Rozycki, J.-F. Qiao, and B. M. Wilamowski, "Nonlinear system modeling using RBF networks for industrial application," *IEEE Trans. Ind. Informat.*, vol. 14, no. 3, pp. 931–940, Mar. 2018.
- [14] S. Chen, S. Yu, J. Lü, G. Chen, and J. He, "Design and FPGA-based realization of a chaotic secure video communication system," *IEEE Trans. Circuits Syst. Video Technol.*, vol. 28, no. 9, pp. 2359–2371, Sep. 2018.
- [15] D. Abbasinezhad-Mood and M. Nikooghadam, "Efficient anonymous password-authenticated key exchange protocol to read isolated smart meters by utilization of extended Chebyshev chaotic maps," *IEEE Trans. Ind. Informat.*, vol. 14, no. 11, pp. 4815–4828, Nov. 2018.
- [16] M. Bakiri, C. Guyeux, J.-F. Couchot, L. Marangio, and S. Galatolo, "A hardware and secure pseudorandom generator for constrained devices," *IEEE Trans. Ind. Informat.*, vol. 14, no. 8, pp. 3754–3765, Aug. 2018.

- [17] A. N. Pisarchik and U. Feudel, "Control of multistability," *Phys. Rep.*, vol. 540, no. 4, pp. 167–218, Jul. 2014.
- [18] J. Ma, F. Wu, G. Ren, and J. Tang, "A class of initials-dependent dynamical systems," *Appl. Math. Comput.*, vol. 298, pp. 65–76, Apr. 2017.
- [19] P. Jin, G. Wang, H. H.-C. Iu, and T. Fernando, "A locally active memristor and its application in a chaotic circuit," *IEEE Trans. Circuits Syst. II, Exp. Briefs*, vol. 65, no. 2, pp. 246–250, Feb. 2018.
- [20] H. Bao, A. Hu, W. Liu, and B. Bao, "Hidden bursting firings and bifurcation mechanisms in memristive neuron model with threshold electromagnetic induction," *IEEE Trans. Neural Netw. Learn. Syst.*, vol. 31, no. 2, pp. 502–511, Feb. 2020.
- [21] Q. Lai, P. D. K. Kuate, F. Liu, and H. H.-C. Iu, "An extremely simple chaotic system with infinitely many coexisting attractors," *IEEE Trans. Circuits Syst. II, Express Briefs*, vol. 67, no. 6, pp. 1129–1133, Jun. 2020.
- [22] Z. T. Zhusubaliyev, E. Mosekilde, and E. V. Pavlova, "Multistability and torus reconstruction in a DC–DC converter with multilevel control," *IEEE Trans. Ind. Informat.*, vol. 9, no. 4, pp. 1937–1946, Nov. 2013.
- [23] H. Bao, M. Chen, H. Wu, and B. Bao, "Memristor initial-boosted coexisting plane bifurcations and its extreme multi-stability reconstitution in two-memristor-based dynamical system," *Sci. China Technol. Sci.*, vol. 63, no. 4, pp. 603–613, Nov. 2019.
- [24] B. Bao, H. Li, H. Wu, X. Zhang, and M. Chen, "Hyperchaos in a second-order discrete memristor-based map model," *Electron. Lett.*, vol. 56, no. 15, pp. 769–770, Jul. 2020.
- [25] Z. Hua, B. Zhou, and Y. Zhou, "Sine chaotification model for enhancing chaos and its hardware implementation," *IEEE Trans. Ind. Electron.*, vol. 66, no. 2, pp. 1273–1284, Feb. 2019.
- [26] T. Prodromakis, C. Toumazou, and L. Chua, "Two centuries of memristors," *Nature Mater.*, vol. 11, no. 6, pp. 478–481, May 2012.
- [27] H. Yang and G.-P. Jiang, "Reference-modulated DCSK: A novel chaotic communication scheme," *IEEE Trans. Circuits Syst. II, Exp. Briefs*, vol. 60, no. 4, pp. 232–236, Apr. 2013.
- [28] M. Liu, S. Zhang, Z. Fan, S. Zheng, and W. Sheng, "Exponential  $H_\infty$  synchronization and state estimation for chaotic systems via a unified model," *IEEE Trans. Neural Netw. Learn. Syst.*, vol. 24, no. 7, pp. 1114–1126, Jul. 2013.
- [29] C. Bandt and B. Pompe, "Permutation entropy: A natural complexity measure for time series," *Phys. Rev. Lett.*, vol. 88, no. 17, Apr. 2002, Art. no. 174102.
- [30] J. Theiler, "Efficient algorithm for estimating the correlation dimension from a set of discrete points," *Phys. Rev. A*, vol. 36, no. 9, pp. 4456–4462, Nov. 1987.
- [31] P. Frederickson, J. L. Kaplan, E. D. Yorke, and J. A. Yorke, "The Liapunov dimension of strange attractors," *J. Differ. Equ.*, vol. 49, no. 2, pp. 185–207, Aug. 1983.
- [32] L. Zhang, Z. Chen, W. Rao, and Z. Wu, "Efficient and secure non-coherent OFDM-based overlapped chaotic chip position shift keying system: Design and performance analysis," *IEEE Trans. Circuits Syst. I, Reg. Papers*, vol. 67, no. 1, pp. 309–321, Jan. 2020.
- [33] A. Akgul, H. Calgan, I. Koyuncu, I. Pehlivan, and A. Istanbullu, "Chaos-based engineering applications with a 3D chaotic system without equilibrium points," *Nonlinear Dyn.*, vol. 84, no. 2, pp. 481–495, Apr. 2016.
- [34] Y. Ma, C. Li, and B. Ou, "Cryptanalysis of an image block encryption algorithm based on chaotic maps," *J. Inf. Secur. Appl.*, vol. 54, Oct. 2020, Art. no. 102566.



**Houzhen Li** (Student Member, IEEE) received the B.S. degree in optoelectronic information science and engineering from the Changshu Institute of Technology, Suzhou, China, in 2019. He is currently working toward the M.S. degree in electronics science and technology with the School of Microelectronics and Control Engineering, Changzhou University, Changzhou, China.

His research interests include memristive neuromorphic circuit, and nonlinear circuits and systems.



**Zhongyun Hua** (Member, IEEE) received the B.S. degree from Chongqing University, Chongqing, China, in 2011, and the M.S. and Ph.D. degrees from the University of Macau, Macau, China, in 2013 and 2016, respectively, all in software engineering.

He is currently an Associate Professor with the School of Computer Science and Technology, Harbin Institute of Technology, Shenzhen, China. His research interests include chaotic system, chaos-based applications, and multimedia security.



**Han Bao** (Student Member, IEEE) received the B.S. degree in landscape design from the Finance and Economics University of Jiangxi, Nanchang, China, in 2015 and the M.S. degree in art and design from Changzhou University, Changzhou, China, in 2018. He is currently working toward the Ph.D. degree in nonlinear system analysis and measurement technology with the Nanjing University of Aeronautics and Astronautics, Nanjing, China.

In 2019, he visited the Computer Science Department, University of Auckland, Auckland, New Zealand. His research interest includes memristive neuromorphic circuit, nonlinear circuits and systems, and artificial intelligence.



**Lei Zhu** received the B.S. degree in mechanical engineering from Yangzhou University, Yangzhou, China, in 2002, and the M.S. degree in optical engineering from Yan'an University, Qinzhuangdiao, China, in 2006.

He is currently an Associate Professor with the School of Electrical and Information Engineering, Jiangsu University of Science and Technology, Zhenjiang, China. His research interest mainly focuses on nonlinear circuits and systems.



**Mo Chen** (Member, IEEE) received the B.S. degree in information engineering, the M.S. degree in electromagnetic field and microwave technology, and the Ph.D. degree in electromagnetic field and microwave technology from Southeast University Nanjing Alumnus Forest, Nanjing, China, in 2003, 2006, and 2009, respectively.

Between 2009 and 2013, she was a Lecturer with Southeast University, Nanjing, China. She is currently an Associate Professor with the School of Microelectronics and Control Engineering, Changzhou University, Changzhou, China. Her research interest includes memristor and its application circuits, and other nonlinear circuits and systems.



**Bocheng Bao** (Member, IEEE) received the B.S. and M.S. degrees in electronic engineering from the University of Electronics Science and Technology of China, Chengdu, China, in 1986 and 1989, respectively, and the Ph.D. degree in information and communication engineering from the Nanjing University of Science and Technology, Nanjing, China, in 2010.

From 2008 to 2011, he was a Professor with the School of Electrical and Information Engineering, Jiangsu University of Technology, Changzhou, China. Then, he was a Full Professor with the School of Microelectronics and Control Engineering, Changzhou University, Changzhou. In 2013, he visited the Department of Electrical and Computer Engineering, University of Calgary, Calgary, AB, Canada. He has more than 20 years experience in the industry and was with several enterprises as Senior Engineer and General Manager. His research interests include bifurcation and chaos, analysis and simulation in neuromorphic circuits, power electronic circuits, and nonlinear circuits and systems.

Dr. Bao was the recipient of The IET Premium Awards in 2018.